The Kaolin and Bentonite Deposit of Tamame De Sayago (Zamora, Spain): Mineralogy, Geochemistry, and Genesis

E. M. Manchado · M. Suárez · E. García-Romero

Abstract A geological, mineralogical, and geochemical characterization of the Tamame de Sayago (Zamora, Spain) deposit was carried out with the aim of knowing the conditions that facilitated the genesis in the same deposit of kaolinite and smectites. The alteration processes affecting a Variscan granite were deduced throughout the study of a very wide group of representative samples by X-ray diffraction (XRD), scanning electron microscopy (SEM), chemical analyses of major, minor, and trace elements, as well as $\delta^{18}O$, $\delta^{34}S$ stable isotope and K/Ar dating analyses. In addition, 2D and 2.5D graphs of the kaolinite and smectite isoconcentrations were obtained from core data. According to the color and texture, two different clayey rock types were identified and named as homogeneous alteration zones (ZAHO) and heterogeneous alteration zones (ZAHE). The ZAHO are regoliths in which the granite texture is preserved, and the feldspars are almost completely kaolinized. In the ZAHE, the original texture of the granitic rock is lost, and the main clay mineral is smectite. The mineralogical composition is similar, with kaolinite, smectite, mica, quartz, scarce feldspar, and occasionally natroalunite and APS (aluminum-phosphate-sulphate); however, the mineral concentration varies considerably because ZAHO are rich in kaolin areas whereas ZAHE are bentonitic areas. Both rock types contain numerous veins and nodules. The weathering of the Paleozoic granite alongside the absence of sedimentation during the Mesozoic led to the formation of kaolinite that is preserved in ZAHO materials. Nonetheless, during the Cretaceous–Tertiary transit, the conditions of tectonic stability varied. Late Variscan faults reactivated which allowed the percolation of Mg- and Ca-rich hydrothermal fluids through the already kaolinized granite, increasing the alteration of the primary silicates and leading to the formation of smectites in ZAHE materials. The amount of smectites is greater closer to the faults. The stable isotopes indicate the meteoric nature of the low-temperature hydrothermal fluids. The K/Ar data obtained from the natroalunite of veins indicate that those hydrothermal fluids circulated in different pulses from 66.4 ± 1.7 to 58.8 ± 1.5 Ma, as a minimum. Those ages are coincident with the first formation stages of the Duero Basin.

E. M. Manchado · M. Suárez
Department of Geology, University of Salamanca, 37008 Salamanca, Spain

E. García-Romero (✉)
Department of Mineralogy and Petrology, Complutense University of Madrid, 28040 Madrid, Spain
e-mail: mromero@ucm.es

E. García-Romero
Geosciences Institute (IGEO), Spanish Research Council and Complutense University (CSIC-UCM), 28040 Madrid, Spain

⚂ Springer

Introduction

Kaolin and bentonite are very important mineral resources, with Spain being a significant producer. Their applications depend on the physicochemical properties of kaolinite and smectites, respectively. The economic importance of both industrial minerals, namely of kaolinites and smectites, is related to their physical and chemical properties, mainly their surface properties and their ability to absorb and/or adsorb various organic and inorganic compounds. Both are laminar clay minerals and have very small particle size (with widths measuring on the micro scale and heights measuring on the nano scale). Thus, the specific surface area varies accordingly. Furthermore, smectites have layer charge and high cation exchange capacity, making them able to react with inorganic and organic polar reagents, principally water (hydration and dehydration), and giving them the capacity to swell, rheological properties, and high plasticity. These two minerals can be utilized in many industrial sectors with broad uses. Kaolin is mainly used in the paper, ceramics, fiberglass, paint, and rubber industries, while bentonite is used mostly as an absorbent material.

After Murray (1988), kaolinite can be formed by weathering reactions (supergene kaolins), hydrothermal alteration during the late stages of pluton cooling (hydrothermal kaolins), or a combination of both. A comprehensive classification of the environments bearing kaolinite is reported by Dill (2016). This classification includes: (1) primary environments of kaolinization such as vein-type deposits, (sub) -volcanic and pyroclastic deposits, skarn to epithermal deposits and granitic rocks and their associate rocks; (2) secondary environments including kaolin in soil, layered residual kaolin deposits, alluvial–fluvial and delta and coal-bearing; and (3) the tertiary environments of kaolinization which are related to diagenesis and very-low-grade metamorphism and contact metamorphism. Conversely, bentonite deposits are associated with volcanogenic and/or sedimentary environments. According to Belousov and Karelina (2022) and Christidis and Huff (2009), most deposits of high-quality bentonite are related to volcanism and are formed under the influence of low-alkaline seawater or hydrothermal fluids. Smectite composition is controlled partially by the parent rock chemistry. However, bentonite deposits in sediments can also occur in salt lakes and sabkha environments. This process is associated commonly with sepiolite–palygorskite minerals. In such a case, trioctahedral smectites are formed, according to Christidis and Huff (2009) and García-Romero and Suárez (2022).

In Spain, kaolin occurs mainly in sedimentary deposits of kaolin-bearing siliceous sands of the Albian Utrillas Facies in the SE of the Iberian Range (NE Iberian Peninsula) (Bauluz et al., 2008, 2021) and is related to the alteration of Variscan granitoids in the northern Iberian Massif (Galicia and Asturias) (Clauer et al., 2015; Galán & Martín-Vivaldi, 1975a, 1975b; Galán et al., 2010, 2016; Manchado, 2012). Conversely, Spanish bentonites are exploited in the following three different areas and stem from different geological origins: (1) Miocene sedimentary deposits from the Tajo Basin (Madrid–Toledo provinces) in the center of the Iberian Peninsula; (2) Miocene deposits from the hydrothermal alteration of volcanic or sub-volcanic rocks from the Cabo de Gata volcanic area (Almería Province) in the southern part of Spain; and (3) Tamame de Sayago (Zamora province) from the hydrothermal alteration of granitic Variscan rocks (García-Romero et al., 2019). The Tamame de Sayago kaolin–bentonite deposit is found in the Sayago region, Zamora province, Spain, (Fig. 1) and belongs to the anatectic Variscan area of the Tormes Dome, which comprises plutonic (mostly equigranular leucogranites) and high-grade metamorphic rocks (various facies of augen gneisses). Two-mica leucogranite, equigranular and fined-grained rocks, are the predominant rocks in the studied area (López Plaza & López-Moro, 2004, López-Plaza et al., 2008; Martínez et al., 1988). The age of these granites is 310–330 Ma (Dias et al., 1988). The Tormes Dome is shaped by the plutono-metamorphic phenomena that accompanied the uplift of the Variscan chain in the region and is affected by the stages of Variscan, Tardivariscan, and Alpine brittle deformation. Antón, (2003) stated that the region has been subjected to brittle deformation ranging from moderate to low intensity from the Permian to the present.

Prior to the end of the Cretaceous, the area was affected by intense weathering under a wet tropical climate that produced a large kaolinitic
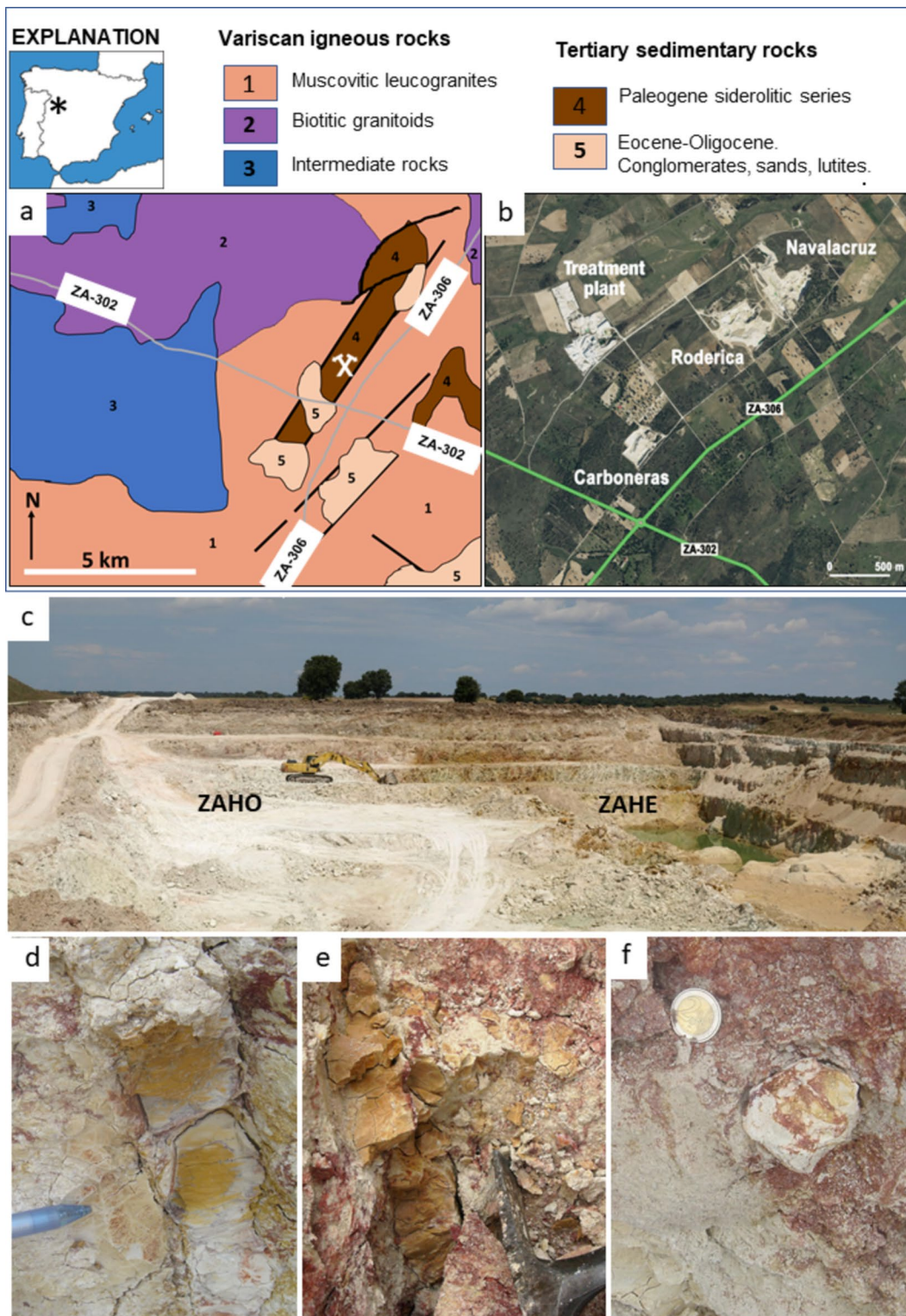
Fig. 1 a Geological scheme and location of the Tamame deposit (indicated with a white quarry symbol). **b** Quarry locations. **c** Navalacruz quarry. The two materials that appear in the deposit, ZAHO and ZAHE, can be distinguished by their colors. **d** Centimetric smectite-rich vein in ZAHO materials. **e** Centimetric smectite rich vein in ZAHE materials. **f** Kaolinite-rich nodule in ZAHO materials

⚛ Springer

mantle (Molina et al., 1990). With the first phase of the Alpine Orogeny, the NE–SW Late Variscan faults were reactivated and tectonic blocks occurred with horsts and grabens affecting the kaolinized granite. The weathering mantle was eroded in the raised blocks, while it was preserved in the sunken blocks because of the Late Cretaceous to Early Paleocene transition sediments covering the kaolinitic materials. Therefore, most of the kaolinitic alteration was dismantled. However, some kaolinized zones in small grabens are still preserved as they were covered by Tertiary material that fossilized and preserved the deposit, as in the case of the studied area, but paleosols are not identified in the zone. Associated with the Alpine tectonic activity, low-temperature silicarich hydrothermal fluids percolated through and significantly altered the rocks. This new alteration of the previously kaolinized granite produced the bentonitization of large areas of the studied deposit according to the preliminary studies conducted by Manchado (2012) and García-Romero et al. (2019).

Exploitation activities in the Tamame de Sayago (Zamora, Spain) deposit, one of the most important kaolin and bentonite deposit in Spain, started in the 1980s. Initially, only kaolin was extracted but nowadays both industrial rocks are mined. The extracted material is classified at the processing plant according to its kaolinite/smectite content and is separated into various commercial products depending on the mineralogical composition. Thus, high-purity kaolin and bentonite are produced as well as some intermediate products, while micas are obtained as a by-product. Bentonite production in Tamame de Sayago increased notably over the last few years. In the current study, a comprehensive mineralogical and geochemical characterization of the Tamame de Sayago deposit was carried out, with the aim of understanding the conditions that facilitated the genesis in the same deposit of two industrial minerals, the formation conditions of which are so different.

Sampling and Analytical Methods

The Tamame de Sayago deposit is mined by strip mining with quarries in three different areas: Navalacruz, located to the north of the deposit; Roderica in the central zone; and Carboneras, the smallest of the three quarries, located to the south of the deposit

(Fig. 1). Overall, 171 representative samples from the quarry fronts were studied from the altered host rocks (64) and small veins and nodules (107).

The mineralogical characterization of the studied samples was conducted by X-ray powder diffraction (XRD), studying raw powdered samples and the < 2 μm fraction obtained after suspension in water and decantation. The clay fraction was studied as oriented aggregates under ambient conditions, after solvation with ethylene glycol, and after heating to 550°C. A Bruker D-8 advance XRD diffractometer using CuKα radiation and a graphite monochromator was employed with a step size of 0.05°2θ and a counting time of 1 s per step. Kaolinite and smectite crystallinity indices were obtained according to the methods proposed by Hinckley (1963) and Biscaye (1965), respectively.

To determine the spatial variation of kaolinite and smectite, 250 data points of mineralogical composition and depth from 31 cores provided by 'Arcillas y Feldespatos Río Pirón Company' were studied. The boreholes were located at the Navalacruz and Roderica quarries, at the north of the deposit. Mineral data and sample depths were studied using the *SURFER 8* software, which allowed 2D and 2.5D graphs of the kaolinite and smectite isoconcentrations to be obtained. The kaolinite and smectite percentages considered for data treatment were the average percentages weighted to the thickness of the altered granite in each borehole. The theoretical variograms from the previously calculated experimental variogram of the two variables considered were modeled prior to studying the spatial variation and obtaining the 2D and 2.5D schemes. The theoretical variograms were the functions representing the variables under study, which allowed the interpolation of unknown data. To draw the 2D and 2.5D maps, point kriging was used as the interpolation method, estimated according to the variogram model that better fitted the experimental variogram. To obtain as real data as possible, a cross-validation was carried out.

A scanning electron microscopy (SEM) study at the Centro Nacional de Microscopía Electrónica in Madrid, Spain, was carried out to observe the textural relationships among restitic and neoformed minerals in a group of representative samples of the various materials identified in the deposit. The samples were air dried, and freshly fractured surfaces were coated with Au in vacuum. The equipment used was

🙋 Springer

a field-emission gun scanning electron microscope JEOL JSM-6335F, operating at 10 and 20 kV and a working distance of 15 mm.

Chemical, stable isotope, and K/Ar dating analyses were carried out at the Activation Laboratory Ltd., Ancaster, Ontario, Canada. Chemical analyses of major, minor, and trace elements were carried out on 56 representative bulk samples of the various depositional lithologies of all quarries. Major and trace elements were measured using 2 g of powdered sample after fusion with lithium metaborate/tetraborate. The molten bead was digested in a weak nitric acid solution. Analysis was done by ICP-OES (Inductively coupled plasma optical emission spectroscopy) and ICP-MS (inductively coupled plasma mass spectrometry). Major elements, along with Sc, Be, V, Sr, Zr, and Ba, were analyzed by ICP-OES and other elements were analyzed by ICP-MS. The chemical index of alteration (CIA, Nesbitt & Young, 1982) was calculated to evaluate the degree of chemical weathering. CIA is a dimensionless number ranging between 0 and 100 that shows the weathering degree of feldspar minerals. $CIA = [Al_2O_3/(Al_2O_3 + CaO + Na_2O + K_2O)] \times 100$. A study of stable isotope $\delta^{18}O$ was carried out on 12 pure silicate samples comprising four kaolinite-rich samples (Nav30, Nav35, Crb6, and Rd43) and eight samples rich in smectite (Nav6, Nav7, Nav11, Nav16, RdF13, RdF17, CrbF11, and Vrd). Furthermore, $\delta^{34}S$ was obtained in four samples rich in alunite (31–64%) (Nav9, Nav9bis, Nav12, and Nav36).

To determine the age of fracture and of the hydrothermal processes that occurred in the deposit, K/Ar analyses were carried out on four selected samples (Nav9, Nav9bis, Nav15, and Nav36) from Navalacruz veins, which had very high alunite concentrations and no muscovite.

Results and Discussion

Mineralogy

The samples were split into four groups according to the field criteria, including texture and color. This classification included two different altered rock types, veins, and nodules. Although the mineralogy found along the deposit is similar, the mineral proportions vary considerably in these four groups. In some areas, the altered rock preserves the granite texture and consists of a regolith where the feldspars are kaolinized almost completely. Manchado (2012) referred to them as ZAHO (Fig. 1b). The ZAHE materials did not preserve the original texture of the granitic rock because of the intense alteration. They consist of highly heterogeneous and fractured clayey rocks, demonstrating great color variations owing to the circulation of iron and manganese oxides. The main clay mineral is smectite, in which the bentonite areas are rich (García-Romero et al., 2019; Manchado, 2012). Usually, ZAHE samples appear as large areas included within ZAHO (Fig. 1b). Three-dimensional relationships between ZAHO and ZAHE are frequently very complex owing not only to the combined effect of the two alteration processes and different fracture stages but also to the slides associated with surface tectonics affecting unconsolidated materials. Contacts between ZAHO and ZAHE can be caused by faults, which are rarely gradual. Typically, ZAHE materials present big bags surrounded by ZAHO with net and irregular contacts (Fig. 1b). Nodules and veins, the thicknesses of which range from millimeters to centimeters, are frequent in both ZAHO and ZAHE (Fig. 1c,d,e).

The mineralogical composition of these four material types, namely, ZAHO, ZAHE, veins, and nodules, is similar because all of them are composed of kaolinite, smectite, micas, quartz, scarce feldspar, and occasionally natroalunite. However, their proportions vary drastically, as revealed by the mean, maximum, and minimum contents of each mineral (Table 1). Predominantly, kaolinitic areas correspond to ZAHO; in these areas, kaolinite concentration reaches 70%, with mean values of 43%, quartz concentration is 25%, and smectite concentration is 18%. In these areas, feldspars are scarce, with mean concentrations of <3%; however, in certain cases they can be found in high concentrations in less altered granites. In certain cases, natroalunite can also appear in very small concentrations. The microstructure of the ZAHO samples observed under SEM is characterized by the presence of mica crystals surrounded by clayey material (Fig. 2a) in which the pseudohexagonal morphology of kaolinite is observed easily at greater magnification (Fig. 2b,c). The sizes of these kaolinite crystals range between 100 nm and several microns. In certain cases, restitic feldspar crystals with their surfaces partially dissolved can be observed, as in Fig. 2d, in

Table 1 Statistical data of mineralogical composition (%)

		Q	F	Al	Sm	K	M	BI	HI
Granite ZAHO n: 35	Max	50	37	6	54	70	35		
	Min	9	0	0	3	8	0		
	Mean	24.54	2.74	0.97	17.89	42.63	10.17	0.83	0.58
	SD	8.12	6.44	6.44	12.86	16.19	7.12	0.14	0.21
Granite ZAHE n: 29	Max	31	5	12	87	42	12		
	Min	3	0	0	19	0	0		
	Mean	18.45	1.34	0.86	60.28	13.48	5.55	0.97	0.39
	SD	7.13	1.37	2.8	16.26	11.61	3.31	0.01	0.21
Veins and nodules included in ZAHO n: 34	Max	32	7	28	92	79	11		
	Min	2	0	0	9	0	0		
	Mean	14.88	1.15	1.94	36.12	40.24	4.26	0.90	0.29
	SD	8.85	1.76	5.01	23.37	24.17	2.74	0.02	
Veins and nodules included in ZAHE n: 73	Max	100	73	28	73	73	14		
	Min	0	0	0	9	0	0		
	Mean	10.87	0.88	13.64	56.04	13.81	2.58	0.93	
	SD	13.68	22.07	22.07	22.35	15.56	3.19	0.06	

Q Quartz, F Feldspars, Al Alunite, Sm Smectite, K Kaolinite, M Mica, BI Biscaye Index, HI Hinckley Index, Max maximum value, Min Minimum value, SD Standard deviation, n Number of analyses

which kaolinite epigenesis on the feldspar surface is noted.

Conversely, ZAHE are bentonitic areas that can host very high concentrations of smectite (87%), with the mean concentration being slightly >60%. The mean concentrations of kaolinite, quartz, micas, and feldspars in ZAHE are less than those in ZAHO. The smectite concentration is greater, owing to the significant impact of the hydrothermal process. As in ZAHO, alunite is found occasionally.

Representative XRD patterns of the ZAHO and ZAHE mineralogical assemblages are shown in Fig. 3. The microstructure observed in ZAHE samples is quite different from those observed in ZAHO samples; furthermore, the mica crystals are altered to a greater extent and exhibit very curved edges (Fig. 2e,f). The clayey material exhibits the typical bentonite texture: laminar crystal aggregates with undulated edges in which it is not possible to observe individual smectite crystals and with frequent edge–face contacts. The co-existence of kaolinite and smectite from the hydrothermal alteration of acid igneous rocks, demonstrating very similar microstructure to the ZAHE materials, was reported by Kadir and Kart (2009).

The vein thicknesses range from millimeters to centimeters (Fig. 1c,d,e), although they are wider in some cases. They appear embedded both in ZAHO and ZAHE and, as for the massive host rocks, kaolinite and smectite are the most abundant components. No pure kaolinite veins were identified. In ZAHO, vein composition is quite similar, hosting large amounts of kaolinite (Fig. 2g) and variable concentrations of smectite, along with minor amounts of natroalunite or primary minerals, while the veins cutting the ZAHE materials have smectite as the most abundant mineral (56% as mean content) and are rich in alunite. Figure 2h shows the image of a smectite–alunite vein in which isometric crystals of alunite ~1 μm long are surrounded by laminar smectite aggregates. The materials referred to here as natroalunite are, in fact, minerals of the APS group (Manchado et al., 2008). These results concur with those reported by Meunier (2005), which state that short hydrothermal pulses favor the formation of low-charge expansive clays (such as the smectites appearing in these veins), while non-expansive species crystallize in systems in which fluids circulate for longer periods. Ultimately, nodules found in the deposit have compositions similar to those of the veins in ZAHE,

@ Springer

being rich in smectite and alunite and with variable concentrations of quartz and kaolinite.

In the samples that were studied, the 060 reflection of phyllosilicates corresponds to a d_{060} spacing of 1.49 Å, both in ZAHE and ZAHO, indicating that all of them are dioctahedral. Moreover, smectites have very high crystallinity (Fig. 3). The calculated mean value of the Biscaye Index (BI) of all the studied samples of the deposit is 0.92. Comparing their BI values, ZAHE samples have slightly greater crystallinity than ZAHO; the greater the percentage of smectites in the sample, the greater its crystallinity (Table 1). However, kaolinite crystallinity is low according to the Hinckley Index (HI), showing the kaolinite from the ZAHO (which was formed by feldspar weathering) to have a greater crystallinity with a mean value of HI = 0.58 and the kaolinite from the veins to have lower crystallinity with HI = 0.29. Kaolinites from ZAHE, which have experienced a greater influence of the hydrothermal process, have lower HI values (0.39) than those from ZAHO.

2D and 2.5D graphics of the deposit were obtained from the study by mean of *SURFER-8* of the bulk data of the borehole provided by 'Arcillas y Feldespatos Río Pirón'. They were obtained by the experimental and theoretical variograms calculated from the core data (Fig. S1a,b) that were used to obtain the isocontents maps (Fig. S1c,d) and the 2.5D (Fig. S1e,f) models of smectite and kaolinite concentrations. Lag is the distance or interval considered for the calculations, which were 25 in all the variograms. The direction of the experimental variogram considered was N140E and the tolerance was 20°; therefore, all the data from the soundings found between N120E and N160E were considered. Subsequently, the isocontent maps were obtained from the variograms using kriging as the interpolation method. Unsampled points were interpolated by point kriging.

The map of the smectite isocontents was calculated from the weighted average percentage of smectite with regards to the thickness of altered granites in each borehole, calculating the experimental and theoretical variograms, as previously stated, and the isocontent map was obtained from the theoretical variogram (Fig. S1a). The weighted average percentage of smectite was an anisotropic variable and the experimental variogram was calculated for a lag direction of N115E with an angular tolerance of 20°. In the boreholes, the smectite values varied from 0 to 64.24% and the average was 20.26%. The maximum value in the scale was 55%; therefore, some values were underrated. The highest weighted percentage values of smectite had a distinct preferential direction, approximately N40E (Fig. S1c). These maxima form two parallel and displaced imaginary lines (Fig. 4). This showed that the smectite origin was related to a main zone of fracture, with direction ~N40E. A higher degree of fracture through two conjugated faults produced a movement (with horizontal displacement ranging from 100 to 200 m) of a central block in this area (Fig. 4). Furthermore, the theoretical variogram model that best fitted the experimental data for the weighted average kaolinite contents was obtained, and the isocontent map was also obtained from the theoretical variogram (Fig. S1b,d, respectively). Similar to the smectite model, the maximum of the theoretical model underestimated the percentage of kaolinites and in the minima they are overestimated. The maximum and minimum kaolinite percentage values obtained from the boreholes were 47.83 and 1.72%, respectively, with a mean value of 26.92% and a standard deviation of 11.73, slightly lower than that of the smectite percentage. The kaolinite distribution is relatively homogeneous in the deposit as in a regolith stemming from the meteoric alteration of the original granitic rock, except for the zone in which the greatest smectite concentrations appear close to fault zones.

Borehole data revealed that the least variability of the deposit is found in the direction N40E. All the diagrams obtained showed a similar trend in this direction, being more evident in the graph corresponding to the smectite distribution. This direction corresponds to the reactivated Late Variscan fractures (Anton, 2003) and, in turn, coincides with that of the faults limiting the deposit. These data allow the deduction that, in the area studied, a N40E-direction fault occurred with the uplifted block to the NW (the base of the tertiary in this area was slightly higher). One could, therefore, deduce that the smectites from the Tamame de Sayago deposit, which present maximum concentrations in the same direction, could have an origin related to this fault related to the circulation of hydrothermal fluids. Two other conjugate faults displace this fault zone and, therefore, the smectite maximums. These faults (both the N40E and the two conjugates) appeared before the sedimentation of the Tertiary. These conclusions are summarized graphically in Fig. 4, and
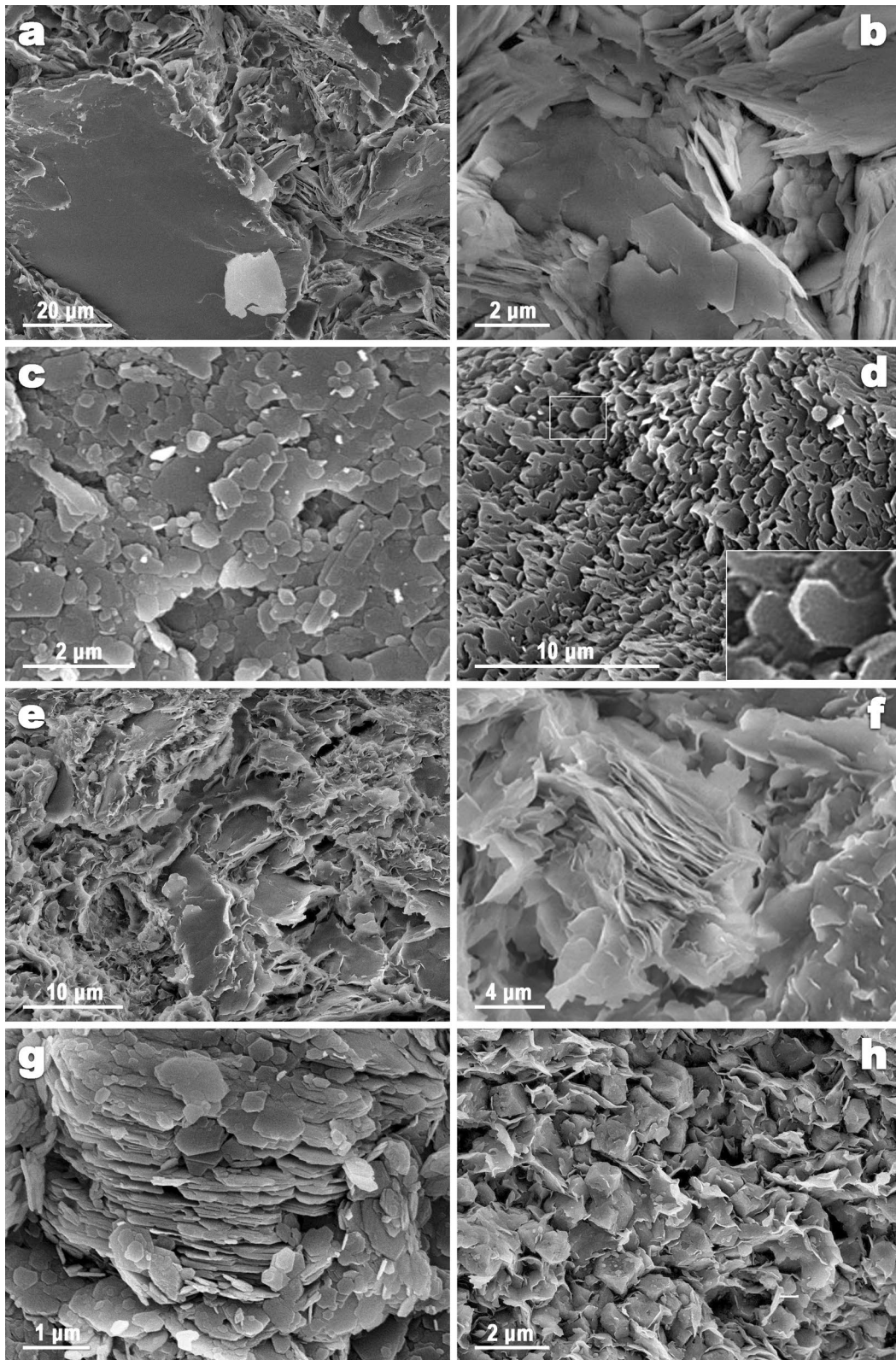
they agree with field observations as the bentonitic zones of ZAHE coincide with the maximum in the isocontents in smectite lines.

Geochemistry

Major element analyses of representative samples show that the most abundant oxides are SiO_2 and Al_2O_3 because they correspond to the mineralogy of rocks that are composed principally of dioctahedral phyllosilicates and quartz (Table S1). The Pearson correlation coefficients (r) among the major elements and the main minerals of the deposit (Table S2) show interesting correlations, in addition to the obvious correlations such as quartz with SiO_2. MgO and CaO are highly correlated with smectites, with r = 0.931 and 0.878, respectively, while natroalunite is correlated with Na_2O (r = 0.857), as expected. Moreover, P_2O_5 (r = 0.744) is in good agreement with the XRD patterns and the presence of some solid solutions with aluminum–phosphate–sulfate (APS) minerals that were referred to in this deposit (García-Romero et al., 2019; Manchado et al., 2008).

Significant variations were found among the ZAHO and ZAHE compositions. SiO_2, MnO, Na_2O,
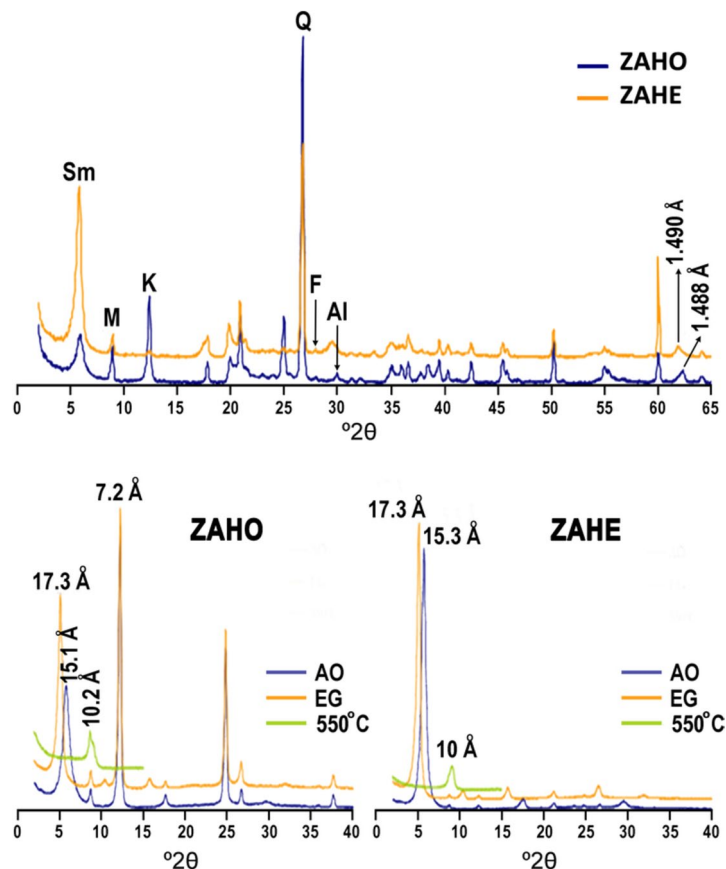

Fig. 3 XRD patterns of representative samples. Upper: powdered samples. Lower: oriented aggregates of the < 2 μm fraction of ZAHO and ZAHE samples where AO is an oriented air-dried aggregate, EG is an oriented aggregate solvated with ethylene glycol, and 550ºC is an oriented aggregate heated at 550ºC for 2 h. Sm = smectite, M = mica, K = Kaolinite, Q = Quartz, F = Feldspar, Al = Natrolunite
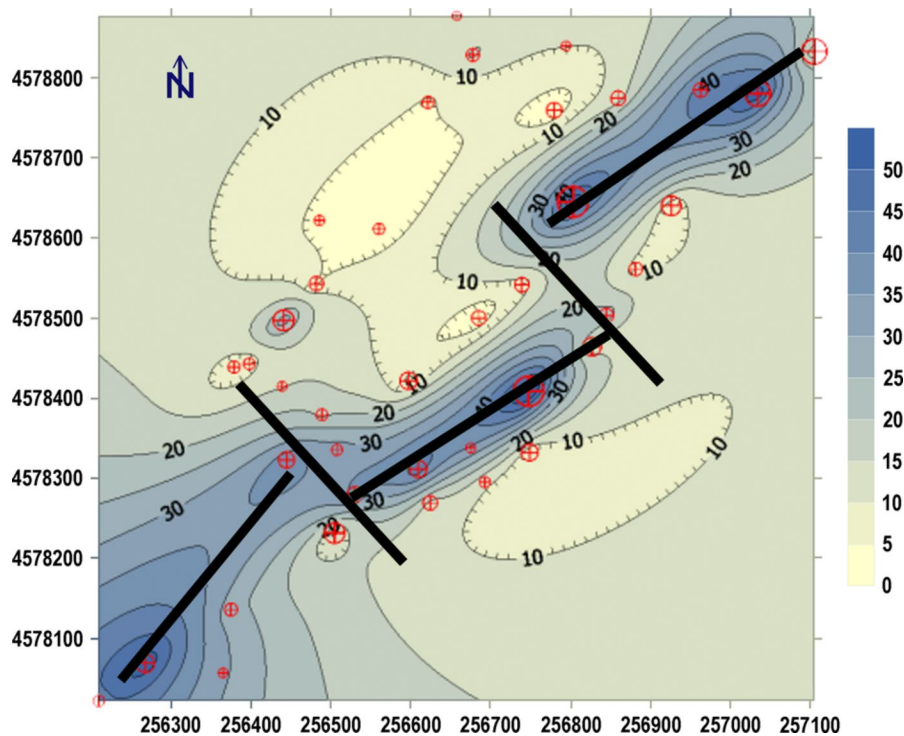
Fig. 4 Deduced fracture zones from the smectite isocontents map. Abscissa and ordinate are UTM (Universal Transversal Mercator) coordinates. Red circles containing crosses indicate the borehole positions. The vertical scale bar indicates the values of smectite isocontents in %

and K$_2$O percentages were similar in ZAHO and ZAHE, the Al$_2$O$_3$ concentration is higher in ZAHO, while Fe$_2$O$_3$, MgO, and CaO were found in greater concentrations in ZAHE (Table 2, Fig. 5). These variations are related to the lower concentrations of kaolinites and the higher smectite concentrations in ZAHE compared to those found in ZAHO. The standard deviations are large (Table 2) because of the material heterogeneity. According to the variations in chemical composition in the clayey materials, the hydrothermal process involved the mobilization of the main octahedral cations of the phyllosilicates and

Ca^{2+} as an exchangeable cation in smectites. A priori, ZAHE materials were expected to host SiO$_2$ concentrations owing to the different crystal chemistry of kaolinites and dioctahedral smectites. Kaolinite, as a 1:1 phyllosilicate, has a smaller amount of silica than smectites, which have a 2:1 layer. However, the mean concentrations of this oxide are very similar in the kaolinitic (ZAHO) and bentonitic (ZAHE) areas. The additional silica needed to transform a 1:1 (kaolinite formed by weathering of the granite) into a 2:1 phyllosilicate (smectite formed by the hydrothermal alteration of the weathered granite) comes from a new

Table 2 Statistical data for the main oxides (%) of the analyzed ZAHO, ZAHE, and veins and nodules

Oxide	SiO$_2$	Al$_2$O$_3$	Fe$_2$O$_3$ (T)	MnO	MgO	CaO	Na$_2$O	K$_2$O	TiO$_2$	P$_2$O$_5$	LOI	Σ
Max	72.99	29.85	10.18	0.094	3.87	11.72	0.94	5.67	0.770	4.04	37.06	101.00
Min	21.91	13.88	0.56	0.002	0.18	0.11	0.05	0.31	0.001	0.02	6.68	98.50
Mean (n: 56)	58.83	19.82	2.06	0.009	1.83	1.48	0.17	1.31	0.229	0.33	13.87	99.94
SD	9.80	4.09	1.44	0.017	1.07	1.84	0.17	1.05	0.175	0.67	6.15	0.65

Max maximum value, Min: Minimum value, SD: Standard deviation, n: Number of analyses

Springer

alteration of the primary minerals, the restitic micas, feldspars, and mainly from quartz, the concentrations of which are lower in ZAHE (Table 2).

The CIA (Nesbitt & Young, 1982) was calculated for the clayey materials of ZAHO and ZAHE. CIA could have a value of 100 when all Ca, K, and Na are leached from the original granite. In the Tamame deposit, the mean value of CIA is 89.31, indicating a high degree of rock alteration. However, significant differences were observed among the ZAHO and ZAHE materials. In ZAHO, the CIA index ranges between 89.62 and 96.69, with 93.21 as the mean. The values obtained for the kaolinitic areas of ZAHO are like those found by Galán et al. (2016), who studied the kaolin from Burela (Spain) and by Bedassa et al. (2019) at the Belessa kaolin (Ethiopia). However, the CIA values in the samples from ZAHE are lower; the mean value is 85.16 and ranges between 69.34 and 88.38. This does not imply that ZAHE are less altered; in fact, it implies just the opposite because the superimposed hydrothermal alteration implies an increase in the Ca content.

When the major element compositions of the samples were normalized with fresh granite data provided by López-Plaza et al. (2008) for the Domo de Tormes pluton in which the deposit is located (Fig. 6), both ZAHO and ZAHE altered granites were significantly depleted in MnO and Na_2O, which was more pronounced in ZAHO than in ZAHE and to a smaller extent in K_2O, Fe_2O_3, and TiO_2. This is because Ca, Na, and K from the K-feldspars and plagioclases were released, in addition to the remobilization of Fe, Ti, and Mn oxides during the weathering. Conversely, ZAHO materials are significantly depleted in MgO and CaO, while they are enriched in ZAHE with regard to the granite. This is because these elements have been remobilized from the weathered granite and concentrated in the ZAHE areas most affected by the hydrothermal process. The main chemical variations that occur in the deposit are related to the degree of alteration, the combined effect of both weathering and hydrothermal processes and element remobilization. According to this comparison, K, Na, Ti, and Mn were lixiviated with the first alteration process, while Mg and Ca were remobilized and concentrated by the hydrothermal fluids. Similar variations were observed in the meteoric alteration of granite by Duddy (1980), Galán et al. (2007), Mongelli (1993), and Panahi et al. (2000).

The chemical composition of veins and nodules is quite similar (Table 2). The SiO_2 percentage is lower than that in altered granites because the quartz concentration is much lower, while Al_2O_3, Na_2O, and especially K_2O are found in high concentrations in veins and nodules and are influenced mainly by the alunite proportions. As for the whole rock, veins from ZAHE are richer in Mg and Ca than veins from ZAHO.

Minor and trace elements (Sc, Be, V, Co, Ga, Rb, Sr, Y, Zr, and Nb) (Fig. S2) for altered granite normalized data with respect to those of fresh granite (López-Plaza et al., 2008) show that, throughout the alteration, enrichment in Sc, V, and Sr has occurred which agrees with observations by Condie et al. (1995) and Galán et al. (2016). Co, Rb, and Be were depleted. According to previous observations, weathered granites lost Rb compared with the fresh rock (Galán et al., 2007, 2016; Mongelli, 1993). Ga remained constant with approximately the same values as those in fresh granite, as in Panahi et al. (2000). Y shows a great variation in ZAHO altered granites and maintains approximately the same concentration values of this element compared to those in fresh granite, while ZAHE show a depletion, as it occurs in the alunite-bearing kaolin deposit of Mudamköy (Kadir et al., 2022).

The values of large-ion lithophile elements, namely Sn, Cs, Ba, Hf, Ta, Tl, Pb, Th, and U normalized with respect to those of fresh granite (Fig. S2), reveal a depletion in Cs and Tl with respect to the concentrations in fresh granite, as was also observed by Galán et al., (2007, 2016). Sn, Ba, and Pb maintain approximately the same concentrations as those in fresh granite or slightly lower. Hf and Ta have similar behavior with analogous values to the fresh granite in ZAHO while in ZAHE they are lower. Panahi et al. (2000) affirmed that Hf is an immobile element under meteoric conditions. The Zn and Ni concentrations in samples are below the detection limit (30 ppm for Zn and 20 for Ni); the deposit samples are depleted in these elements with respect to the concentrations in the fresh granite, in good agreement with Turekian (1978) who affirmed that Ni is mobilized easily during the weathering process.

REE analyses are also normalized with respect to the values obtained by López-Plaza et al. (2008) (Fig. S2). Most samples from ZAHO are enriched in REEs while those from ZAHE show very different
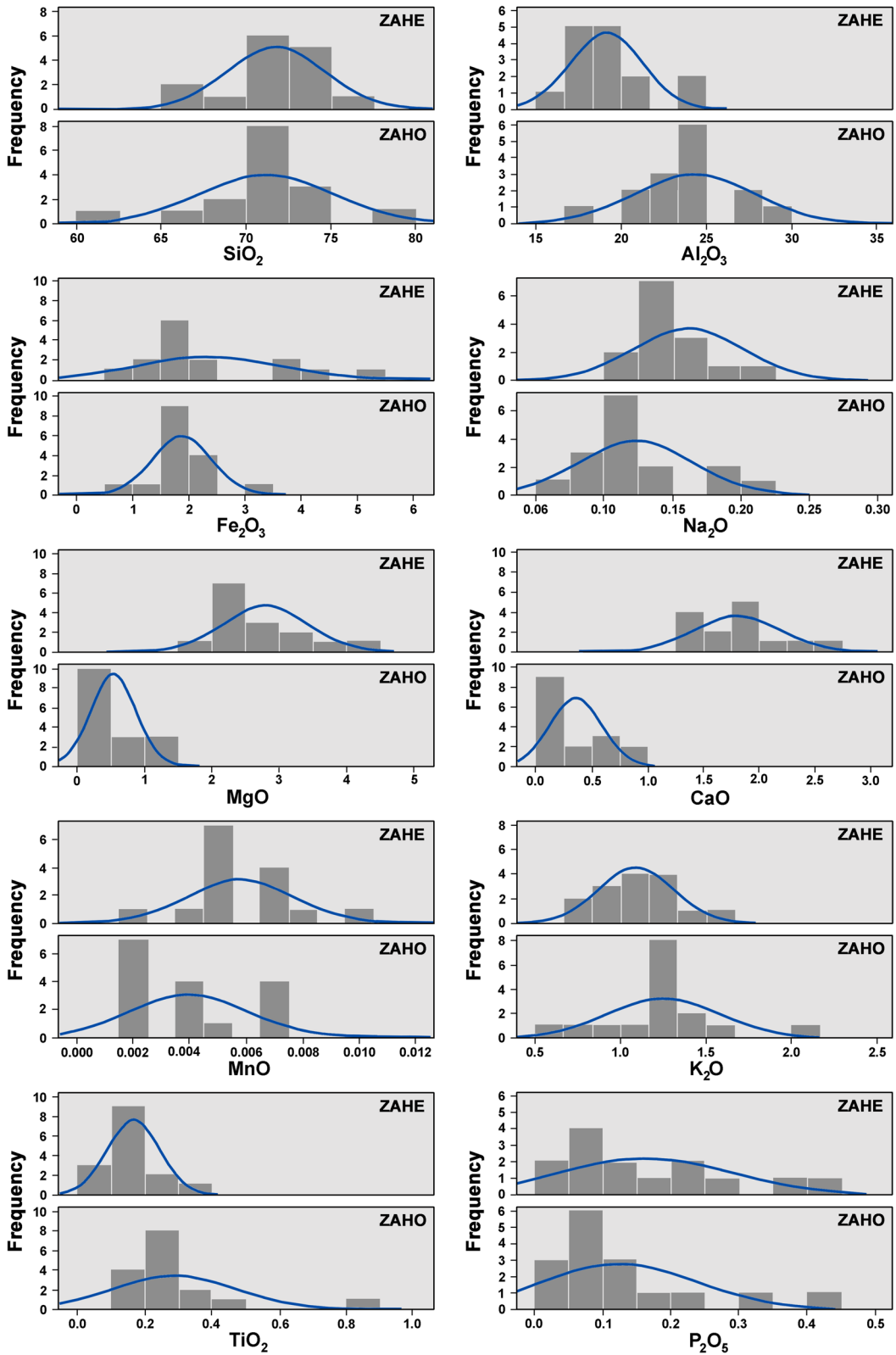
◄**Fig. 5** Histograms of major element contents (% oxide) of representative samples from ZAHO and ZAHE materials. The relative enrichment in Mg and Ca of ZAHE relative to ZAHO can be observed. ZAHO: Homogeneous alteration zones. ZAHE: Heterogeneous alteration zones

concentrations, although most of them present normalized values of <1. The samples from veins of ZAHE from Navalacruz quarry show notable impoverishment in Tm (below the detection limit). Therefore, a certain fractionation of HREE would be more immobile, but not of the LREEs.

Nesbitt (1979), Duddy (1980), Middleburg et al. (1988), Marsh (1991), Prudencio et al. (1993), Mongelli (1993), and Morey and Setterholm (1997) studied systems in which weathering caused REE mobilization and fractionation. Thus, the results of Nesbitt (1979) and Duddy (1980) indicated that the REEs are redistributed within the profile of meteoric alteration; i.e. no element gains or losses occur when considering the entire profile of meteoric alteration. Nesbitt (1979) justified general variations in the profile with respect to the original rock, considering that part of the profile may have been eroded. However, other authors justified the REE fractionation, emphasizing that they form more soluble complexes than LREEs (Cantrell & Byrne, 1987, among others). Thus, Mongelli (1993) verified that in the meteoric alteration of granite, the LREEs show a greater tendency to concentrate than the HREEs, which is partially because a greater solubility of the HREEs is favored by being in non-acids.

Stable Isotope Analysis $\delta^{18}O$ and $\delta^{34}S$

Stable isotope analysis of $\delta^{18}O$ and $\delta^{34}S$ was carried out in 12 representative samples that contain exclusively silicate minerals and in four samples with the highest alunite contents, respectively. The $\delta^{18}O$ values were compared with the Mean Ocean Water Standard range between 17.5 and 25.8‰, with significant differences among samples derived from ZAHO, ZAHE, and veins (Fig. 7). In any case, these $\delta^{18}O$ values are similar to those obtained by Savin and Epstein (1970) for kaolin from Arkansas and South Carolina (~20‰), by Clauer et al. (2015) for the kaolin deposits from weathered Variscan granitoids of Galicia (16.5–22.4‰), and by Galán et al. (2016) (19.8–21.0‰) from the Burela (Spain) kaolin deposit. Those authors found that these values were consistent with a supergene origin, indicating that the most likely scenario was that formation occurred in equilibrium with meteoric waters at near surface temperatures (between 15 and 36ºC). However, these values are high compared with those in fresh granite proposed by Faure (1977) for S type granites (from 13 to 18‰) and those obtained by López-Plaza et al. (2008) for the unaltered granite in the Tamame area (12.9‰). According to Murray and Janssen (1984), when kaolins have a hydrothermal origin, the $\delta^{18}O$ values range between 15 and 19‰, whereas kaolins from weathered igneous rocks range between 2 and 14‰. Finally, sedimentary kaolins demonstrate the highest values with $\delta^{18}O > 19$‰. Only three of the samples from the Tamame deposit have values that correspond to kaolins from weathered granites, and
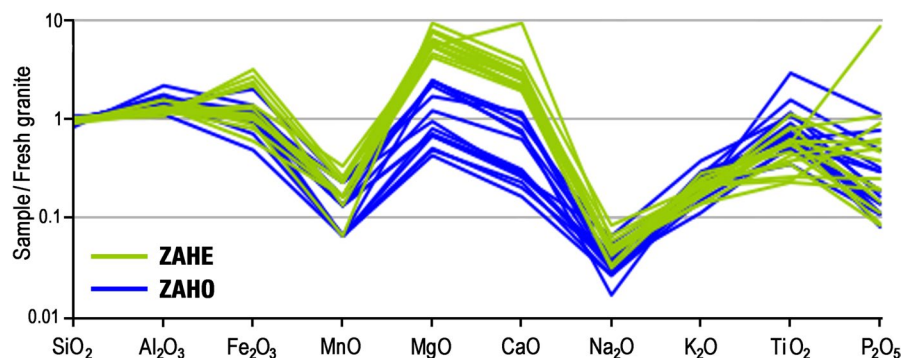

Fig. 6 Representation of the contents of the major elements, as oxides, normalized to the regional fresh granite (López-Plaza et al., 2008)
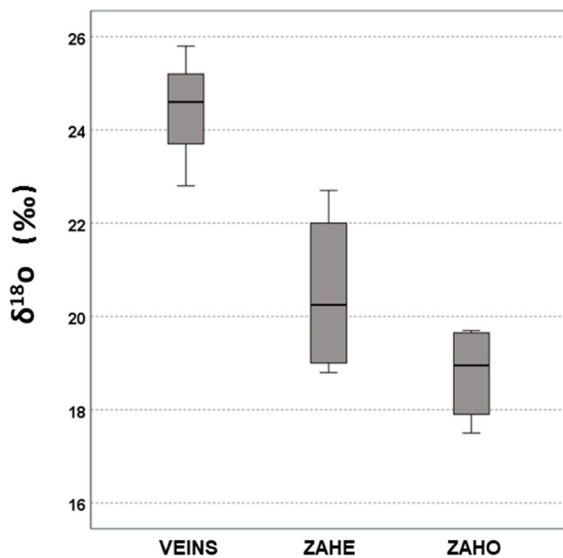
Fig. 7 Box diagram with the $\delta^{18}O$ values grouped by sample type: ZAHO and ZAHE materials and veins. ZAHO: Homogeneous alteration zones. ZAHE: Heterogeneous alteration zones

the other samples have values >19‰. This is due to the fact that the isotopic signal in these materials is related to the circulation of surface waters that percolate and then go up through fractures. According to that, the highest values are those of veins (24.5‰). In the kaolin deposits of western Sardinia (Italy), Simeone et al. (2005) found $\delta^{18}O$ values ranging between 16.6 and 21.4‰ for clayey rocks formed from steam-heated meteoric waters.

The samples analyzed for $\delta^{34}S$ were all derived from ZAHE veins; they do not have restitic minerals and S is present only in alunite. The values obtained are referred to Canyon Diablo Troilite and range between 12.8 and 13.5‰. The mean analyzed value of $\delta^{34}S$ was 13.2‰. Dill (2001) proposed $\delta^{34}S$ values for alunite of hydrothermal origin that range between 16 and 28‰; for alunite of supergene origin, values between 4 and 10‰; and for alunite of evaporitic origin the $\delta^{34}S$ ranges from 11 to 15‰. Bird et al. (1990) obtained $\delta^{34}S$ values of between 1.5 and 6.9‰ in alunite formed in a supergene environment with a sulfate derived from the marine cycle. According to this, Field and Lombardi (1972) determined the supergene origin of alunite with $\delta^{34}S$ values ranging between 5.5 and 6.3‰,

and higher $\delta^{34}S$ values corresponding to hydrothermal waters. The values found in the Tamame samples are not typical of meteoric water because they are too high. They are clearly far from the $\delta^{34}S$ values corresponding to the marine environment and do not reach the values of hydrothermal waters. This observation can be explained, as for oxygen isotopes, by the fluids coming from meteoric waters that percolated through the weathered granite, enriching themselves with the most mobile elements, to later ascend through fractures and precipitate into new minerals (smectite and alunite), then percolate again through the granite, modifying its mineralogical composition in a low-temperature hydrothermal process.

K/Ar Geochronology

Four samples from veins with high alunite concentration and no mica, which ensures that the age obtained is not influenced by this restitic mineral, were chosen for dating the fracture process (Table S3). The ages obtained ranged between the Maastrichtian (Upper Cretaceous) and the Selandian (Paleocene) (Fig. 8). The veins analyzed were formed between 66.4 ± 1.7 and 58.8 ± 1.5 Ma, indicating their formation in several hydrothermal pulses. Considering the measurement errors, the Nav9bis and Nav36 samples may correspond to the same process at ~59 Ma. These results indicate that the meteoric alteration was prior to 66.4 ± 1.7 Ma and that the Tertiary sediments covering the deposit were formed after 58.8 Ma, and in the middle, three fracture steps occurred at least. These results agree with those reported by Meunier (2005) when he stated that short hydrothermal pulses favor the formation of low-charge expansive clays (such as the smectites that appear in these veins), while non-expansive species crystallize in systems in which fluids circulate for longer periods.

The ages obtained coincide with the first stages of formation of the Duero Basin, in which the deposit located at the western edge occurred in the uppermost Cretaceous–Paleogene time according to Molina et al. (1990) and Granados et al. (2012). The first sediments in the southeast areas of the basin could be Maastrichtian in age.
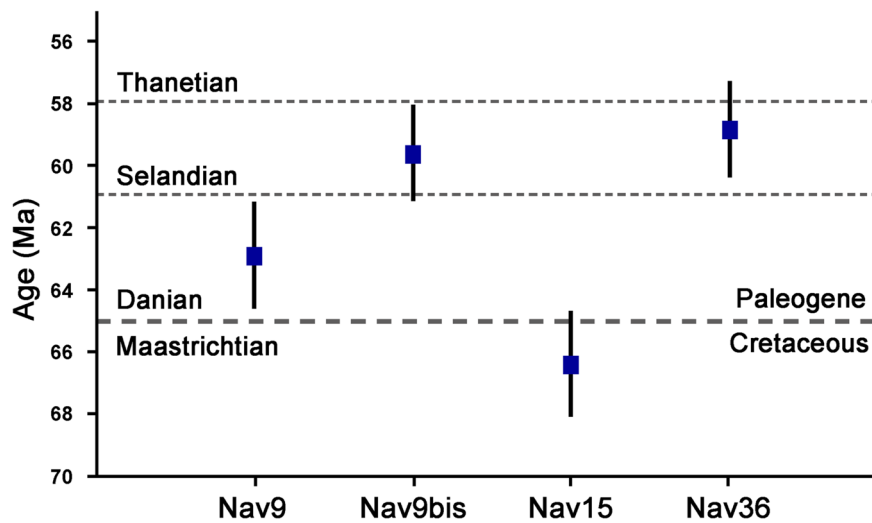
Fig. 8 Box diagram with the ages of representative samples of veins dated by K/Ar geochronology

Conclusions

The kaolin–bentonite deposit of Tamame de Sayago is the result of the combined effect of weathering and hydrothermal processes that altered the primary granite minerals and gave rise to clay mineral neoformation. During most of the Mesozoic, the absence of sedimentation and the humid tropical climate led to the formation of an important lateritic alteration mantle (Martín-Serrano, 1988). The weathering of the Paleozoic granite, which is assumed to be analogous to that studied by López-Plaza et al. (2008), gave rise to the ZAHO materials very rich in kaolinite. Weathering caused the depletion of Fe, Mn, Ca, Na, K, Ti, P, Be, Co, Zn, Rb, Cs, Tl, and Th and the concentration or relative enrichment of Al, Sc, Sr, Nb, and Sn.

In the Cretaceous–Tertiary transition, the conditions of tectonic stability and humid tropical climate varied, specifically during the Laramic phase of the Alpine orogeny. The reactivation of Late Variscan faults affected the alteration mantle of the Variscan plinth (Santisteban Navarro, 1998) and led to a complicated paleotopography of horst–graben systems. Fluid circulation through the fractures affected large areas and gave rise to bentonitized ZAHE materials. Low-temperature hydrothermal fluids, rich in Mg and Ca, percolated through the weathered granite, increasing the alteration of the primary silicates (feldspar, mica, and quartz) and leading to massive

smectite formation and occasional natroalunite and APS. Veins in ZAHE were also rich in Mg and Ca, although they also contain Na, K, P, Sc, Sr, Ba, LREE, Pb, and U. The chemical analyses indicated that the hydrothermal fluids did not contribute new elements to the system but rather that they remobilized some elements in the weathered granite.

The stable isotope results and the regional geology of the area, which excludes the contribution of magmatic waters, indicate that the nature of the low-temperature hydrothermal fluids was meteoric. The meteoric water percolated through the weathered granite, leaching the most mobile elements that were concentrated at depth, increasing their temperature slightly to ascend later through the fractures. Hydrothermal fluid circulation occurred in different pulses between 66.4 ± 1.7 and 58.8 ± 1.5 Ma, at least. The chemical composition of the hydrothermal fluids varied over time. The first veins were richer in kaolinite and the composition changed to alunite–APS minerals, smectites, and kaolinite traces. Alunite was formed from low pH (0.8–5.3) sulfated fluids (Hikov et al., 2010a, 2010b). APS minerals required high PO_4^{3-} activity and a wider pH range (3–8) (Ripp et al., 1998), compatible with smectite formation and at temperatures that could be as low as ~40ºC (Harder, 1972, 1976; Kloprogge et al., 1977), in line with the heating produced by the geothermal gradient affecting infiltrated meteoric waters. The nature of the fluids changed,

both in chemical composition and pH, becoming more basic and giving rise to the formation of very rich or pure smectite veins. According to the stability diagrams of kaolinite at various temperatures and in the presence of dissolved Fe^{2+} and Mg^{2+} as proposed by Dill (2016), smectite could form from kaolinite at temperatures from 100ºC with lower Al^{3+} activity than for ambient temperature and at slightly acid pH. The hydrothermal fluids percolating through the weathered granite partially transformed kaolinite into a dioctahedral smectite, and the amount of this neoformed mineral is higher closer to the faults (Fig. 4).

Authors' contributions Manchado: Experimental and data obtention. Data elaboration.

Suárez: Data elaboration. Writing – reviewing and editing.

García-Romero: Data elaboration. Writing – reviewing and editing.

Declarations

Conflicts interests The authors declare that they have no conflict of interest and approve the publication ethics.

References

Antón, L. (2003). Análisis de la fracturación en un área granítica intraplaca: El Domo de Tormes. *PhD. Thesis, Univ. Complutense de Madrid, 195 pp.*

Bauluz, B., Mayayo, M. J., Laita, E., & Yuste, A. (2021). Micro- and nanotexture and genesis of Ball Clays in the Lower Cretaceous (SE Iberian Range, NE Spain). *Minerals, 11*, 1339. https://doi.org/10.3390/min11121339

Bauluz, B., Mayayo, M. J., Yuste, A., & González López, J. M. (2008). Genesis of kaolinite from Albian sedimentary deposits of the Iberian Range (NE Spain): Analysis by XRD, SEM and TEM. *Clay Minerals, 43*, 459–475.

Bedassa, G., Getaneh, W., & Hailu, B. (2019). Geochemical and mineralogical evidence for the supergene origin of kaolin deposits – Central Main Ethiopian Rift. *Journal of African Earth* Sciences, 143–153.

Belousov, P. E., & Karelina, N. D. (2022). Volcano-sedimentary and hydrothermal bentonite deposits. *Journal of Volcanology and Seismology, 16*(6), 451–461. https://doi.org/10.1134/S0742046322060021

Bird, M. I., Chivas, A. R., & McDougall, I. (1990). An isotope study of surficial alunite in Australia: 2. Potassium–argón geochronolgy. *Chemical Geology, 80*, 133–145.

Biscaye, P. E. (1965). Mineralogy and Sedimentation of recent deep-sea clay in the Atlantic Ocean and adjacent seas and oceans. *Geological Society of America Bulletin., 76*(7), 803–832.

Cantrell, K. J., & Byrne, R. H. (1987). Rare earth element complexation by carbonate and oxalate ions. *Geochimica et Cosmochimica Acta*, 5l, 597–606.

Christidis, G. E., & Huff, W. D. (2009). Geological aspects and genesis of bentonites. *Elements, 5*(2), 93–98. https://doi.org/10.2113/gselements.5.2.93

Clauer, N., Fallick, A. E., Galán, E., Aparicio, P., Miras, A., Fernández-Caliani, J. C., & Aubert, A. (2015). Stable isotope constraints on the origin of kaolin deposits from Variscan granitoids of Galicia (NW Spain). *Chemical Geology, 417*, 90–101.

Condie, K. C., Dengate, J., & Cullers, R. L. (1995). Behavior of rare earth elements in a paleoweathering profile on granodiorite in the Front Range, Colorado, USA. *Geochimica Et Cosmochimica Acta, 59*(2), 279–294.

Dias, G., Leterrier, J., Mendes, A., Simões, P. P., & Bertrand, J. M. (1988). U-Pb zircon and monazite geochronology of post-collisional Hercynian granitoids from the Central Iberian Zone (Northern Portugal). *Lithos, 45*(1–4), 349–369.

Dill, H. G. (2016). Kaolin: Soil, rock and ore: rom the mineral to the magmatic, sedimentary and metamorphic environments. *Earth Science Reviews*, 161(3–4). https://doi.org/10.1016/j.earscirev.2016.07.003.

Dill, H. G. (2001). The geology of aluminium phosphates and sulphates of the alunite group minerals: A review. *Earth-Science Reviews, 53*, 35–93.

Duddy, I. R. (1980). Redistribution and fractionation of rare-earth and other elements in a weathering profile. *Chemical Geology, 30*, 363–381.

Faure, G. (1977). Principles of isotope geology. *John Wiley & Sons, Inc. (Ed). EEUU. 589 pp.*

Field, C., & Lombardi, G. (1972). Sulfur isotopic evidence for the supergene origin of alunita deposits, Tolfa District, Italy. *Mineralium Deposita, 7*, 113–125.

Galán, E., Aparicio, P., Fernández-Caliani, J. C., Miras, A., Márquez, M. G., Fallick, A. E., & Clauer, N. (2016). New insights on mineralogy and genesis of kaolin deposits: The Burela kaolin deposit (Northwestern Spain). *Applied Clay Science, 131*, 14–26.

Galán, E., Fernández-Caliani, J. C., Aparicio, P., Miras, A., & Márquez, M. G. (2010). Mineralogical and geochemical constraints on the origin of the residual kaolin deposits derived from Variscan granitoids of Galicia (Spain). *SME Annual Meet and Exhibit, 2010*, 180–186.

Galán, E., Fernández-Caliani, J. C., Miras, A., Aparicio, P., & Márquez, M. G. (2007). Residence and fractionation of rare earth elements during kaolinization of alkaline peraluminous granites in NW Spain. *Clay Minerals, 42*, 341–352.

Galán, E., & Martín-Vivaldi, J. L. (1975a). Caolines españoles. Geología, mineralogía y génesis. Parte VII. Depósitos hidrotermales. *Boletín De La Sociedad Española De Cerámica y Vidrio, 14*, 123–144.

Galán, E., & Martín-Vivaldi, J. L. (1975b). Caolines españoles. Geología, mineralogía y génesis. Parte VIII. Depósitos residuales y volcánicos. *Boletín De La Sociedad Española De Cerámica y Vidrio, 14*, 351–370.

García-Romero, E., Manchado, E., Suárez, M., & García-Rivas, J. (2019). Spanish Bentonites: a Review and new data on their geology, mineralogy, and crystal chemistry. *Minerals, 9*, 696. https://doi.org/10.3390/min9110696

García-Romero, E., & Suárez, M. (2022). HRTEM evidence of Tajo Basin mineralogical complexity: Crystal chemistry and genetic relationship. *Applied Clay Science, 224*, 106515. https://doi.org/10.1016/j.clay.2022.106515

Granados, P., Ferrer, O., Butillé, M., Muñoz, J. A., Roca, E., Ballesteros, J. C., Giménez, A., Vallejo, R. A., & Gonzále, P. (2012). 3D geometry, structure, and formation of the Duero basin within the Pyrenean Orogen geodynamic scenario. *Geotemas, 13*, 517–520.

Harder, H. (1972). The role of magnesium in the formation of smectite minerals. *Chemical Geology, 10*, 31–39.

Harder, H. (1976). Nontronite synthesis at low temperatures. *Chemical Geology, 18*, 169–180.

Hikov, A., Lerouge, C., & Velinova, N. (2010b). Geochemistry of alunite group minerals in hydrothermally altered rocks from the Asarel porphyry copper deposit, Central Srednogorie. Bulgarian Geological Society, National Conference with international participation "GEOSCIENCES 2010b", 18–19.

Hikov, A., Lerouge, N., & Velinova,. (2010). Geochemistry of alunite group minerals in advanced argillic altered rocks from the Asarel porphyry copper deposit, Central Srednogorie. *Reviews of the Bulgarian. Geological Society, 71*(1–3), 133–148.

Hinckley, D. N. (1963). Variability in "Crystallinity" values among the kaolin deposits of the Coastal Plain of Georgia and South Carolina. *Clays and Clay Minerals, 11*, 229–235.

Kadir, S., Atres, H., Erkoyun, H., Külaj, T., & Esenli, F. (2022). Genesis of alunite-bearing kaolin deposit in Mudamköy member of the Miocene Göbel Formation, Mustafakemalpaşa (Bursa), Turkey. *Apply Clay Science, 221*, 106407.

Kadir, S., & Kart, F. (2009). The occurrence and origin of the Söğüt kaolinite deposits in the Paleozoic Saricakaya granite-granodiorite complexes and overlying Neogene sediments (Bilecik, Northwestern Turkey). *Clays and Clay Minerals, 57*(3), 311–329.

Kloprogge, T., Komarneni, S., & Amonette, J. E. (1977). Synthesis of smectite clay minerals: A critical review. *Clays and Clay Minerals, 47*, 529–554.

López Plaza, M., & López-Moro, F. J. (2004). El Domo de Tormes. In J. A. Vera (Ed.), *Geología de España* (pp. 100–101). SGE-IGME.

López-Plaza, M., López-Moro, F. J., Vicente-Tavera, S., & Vicente-Villardón, J. L. (2008). Los leucogranitos equigranulares del Domo de Tormes (Zona Centro Ibérica): discriminación geoquímica mediante Biplot Canónico y significado petrogenético. *E-Terra*, 5 – nº4.

Manchado, E. M. (2012). Arcillas Especiales de Tamame de Sayago (Zamora): Mineralogía, Génesis y Propiedades. *PhD thesis, Univ. Salamanca, Spain*, pp. 526.

Manchado, E. M., Suárez, M., & García-Romero, E. (2008). Minerales del grupo de la alunita en el yacimiento de caolinita de Tamame de Sayago (Zamora). *Macla, 9*, 151–152.

Marsh, J. S. (1991). REE fractionation and Ce anomalies in weathered Karoo dolerite. *Chemical Geology, 90*, 189–194.

Martínez, F. J., Julivert, M., Sebastián, A., Arboleda, M. L., & Gil-Ibarguchi, J. I. (1988). Structural and thermal evolution of metamorphism. In R. D. Dallmeyer & E. Martínez García (Eds.), *Pre-Mesozoic Geology of Iberia* (pp. 207–211). Springer-Verlag.

Martín-Serrano, A. (1988). El relieve de la región occidental zamorana. La evolución geomorfológica de un borde del Macizo Hespérico. *Instituto de Estudios Zamoranos Florián de Ocampo, Diputación de Zamora*. pp. 306.

Meunier, A. (2005). *Clays*, pp. 1–472. https://doi.org/10.1007/b138672.

Middleburg, J. J., Van der Weijden, C. H., & Woittiez, J. R. W. (1988). Chemical processes affecting mobility of major, minor and trace elements weathering of granitic rocks. *Chemical Geology, 68*, 253–273.

Molina, E., Cantano, M., Vicente, M. A., & García Rodríguez, P. (1990). Some aspects of paleoweathering in the Iberian Hercynian Massif. *CATENA, 17*, 333–346.

Mongelli, G. (1993). REE and other trace elements in a granitic weathering profile from "Serre", Southern Italy. *Chemical Geology, 103*, 17–25.

Morey, G. B., & Setterholm, D. R. (1997). Rare earth element in weathering profiles and sediments of Minnesota: Implications for provenance studies. *Journal of Sedimentary Research, Sec A, 67*, 105–115.

Murray, H. H., & Janssen, J. (1984). Oxygen isotopes – indicators of kaolin genesis? *Proceeding of the 27th International Geological Congress Moscow*, 287–304.

Murray, H. H. (1988). Kaolin minerals: their genesis and occurrences. In S. W. Bailey (Ed.), *Hydrous Phyllosilicates, Reviews in Minerals* (Vol. 19, pp. 67–89). Washington, DC: Mineralogical Society of America.

Nesbitt, H. W. (1979). Mobility and fractionation of rare earth elements during weathering of a granodiorite. *Nature, 279*, 206–210.

Nesbitt, H. W., & Young, G. M. (1982). Early Proterozoic climates and past plate motions inferred from major element chemistry of lutites. *Nature, 299*, 715–717.

Panahi, A., Young, G. M., & Rainbird, R. H. (2000). Behavior of major and trace elements (including REE) during Paleoproterozoic pedogenesis and diagenetic alteration

of an Archean granite near Ville Marie, Québec Canada. *Geochimica Et Cosmochimica Acta, 64*(13), 2199–2220.

Prudencio, M. I., Braga, M. A. S., & Gouveia, M. A. (1993). REE mobilization, fractionation and precipitation during weathering of basalt. *Chemical Geology, 107*, 251–254.

Phosphate mineralization in metamorphosed high-alumina rocks of Ichetuyskoe ore occurrence (south-west Transbaikali). *Proceedings of the Russian Mineralogical Society, 127*(6), 98–108 (in Russian with an English abstract).

Santisteban Navarro J. I. (1998). El drenaje del SO de la Cuenca del Duero durante el Paleógeno superior y Neógeno. *PhD thesis. Univ. Complutense. Madrid, Spain.*

Savin, S. M., & Epstein, S. (1970). The oxygen and hydrogen isotope geochemistry of clay minerals. *Geochimica Et Cosmochimica Acta, 34*, 25–42.

Simeone, R., Dilles, J. H., Padalino, G., & Palomba, M. (2005). Mineralogical and stable isotope studies of kaolin deposits: Shallow epithermal systems of western Sardinia, Italy. *Economic Geology, 100*(1), 115–130.

Turekian, K. K. (1978). Nickel - Behaviour during weathering. In K. H. Wedepohl (ed), *Handbook of Geochemistry*, Vol. II, Sect. 28-G-1, Springer.

Ⓓ Springer